SPECIAL
State of the Science of Precipitation
COLLECTION

A Prototype WRF-Based Ensemble Data Assimilation System for Dynamically Downscaling Satellite Precipitation Observations

DUSANKA ZUPANSKI*

CIRA/Colorado State University, Fort Collins, Colorado

SARA Q. ZHANG

NASA Goddard Space Flight Center, Greenbelt, Maryland

MILIJA ZUPANSKI

CIRA/Colorado State University, Fort Collins, Colorado

ARTHUR Y. HOU

NASA Goddard Space Flight Center, Greenbelt, Maryland

SAMSON H. CHEUNG

University of California, Davis, Davis, California

(Manuscript received 12 January 2010, in final form 23 August 2010)

ABSTRACT

In the near future, the Global Precipitation Measurement (GPM) mission will provide precipitation observations with unprecedented accuracy and spatial/temporal coverage of the globe. For hydrological applications, the satellite observations need to be downscaled to the required finer-resolution precipitation fields. This paper explores a dynamic downscaling method using ensemble data assimilation techniques and cloud-resolving models. A prototype ensemble data assimilation system using the Weather Research and Forecasting Model (WRF) has been developed. A high-resolution regional WRF with multiple nesting grids is used to provide the first-guess and ensemble forecasts. An ensemble assimilation algorithm based on the maximum likelihood ensemble filter (MLEF) is used to perform the analysis. The forward observation operators from NOAA–NCEP's gridpoint statistical interpolation (GSI) are incorporated for using NOAA–NCEP operational datastream, including conventional data and clear-sky satellite observations. Precipitation observation operators are developed with a combination of the cloud-resolving physics from NASA Goddard cumulus ensemble (GCE) model and the radiance transfer schemes from NASA Satellite Data Simulation Unit (SDSU). The prototype of the system is used as a test bed to optimally combine observations and model information to produce a dynamically downscaled precipitation analysis. A case study on Tropical Storm Erin (2007) is presented to investigate the ability of the prototype of the WRF Ensemble Data Assimilation System (WRF-EDAS) to ingest information from in situ and satellite observations including precipitation-affected radiance. The results show that the analyses and forecasts produced by the WRF-EDAS system are comparable to or better than those obtained with the WRF-GSI analysis scheme using the same set of observations. An experiment was also performed to examine how the analyses and short-term forecasts of microphysical variables and dynamical fields are influenced by the assimilation of precipitation-affected radiances. The results highlight critical issues to be addressed in the next stage of development such as model-predicted hydrometeor control variables and associated background error covariance, bias estimation, and correction in radiance space, as well as the observation error statistics. While further work is needed to optimize the performance of WRF-EDAS, this study establishes the viability of developing a cloud-scale ensemble data assimilation system that has the potential to provide a useful vehicle for downscaling satellite precipitation information to finer scales suitable for hydrological applications.

* Current affiliation: Precision Wind, Inc., Boulder, Colorado.

Corresponding author address: Sara Q. Zhang, NASA Goddard Space Flight Center, Code 610.1, Greenbelt, MD 20771.
E-mail: sara.q.zhang@nasa.gov

DOI: 10.1175/2010JHM1271.1

© 2011 American Meteorological Society

1. Introduction

Hydrological forecasts for floods and landslides often require precipitation information at finer space and time scales than those available from spaceborne microwave observations. Statistical approaches have been used commonly to merge and downscale precipitation observations (Huffman et al. 2007). There is an emerging interest in using data assimilation techniques to extract information from multiple data sources, combining with high-resolution modeling to downscale satellite observations with dynamic consistency.

However, assimilation of satellite precipitation-affected observations into numerical weather prediction (NWP) models posts special challenges, due to the difficulties in incorporating cloud physics and the precipitation process into observation operators in the data assimilation procedures and in estimating the forecast error covariance in cloudy and precipitation regions. Because of these difficulties, it has been a common practice in operational weather centers to assimilate clear-sky (or cloud-cleared) radiances. Cloud clearing, however, results in discarding important information about clouds and precipitation contained in the cloudy visible, infrared (IR), and microwave radiances (e.g., Andersson et al. 2005; Errico et al. 2007). An example, shown in Fig. 1, illustrates that the standard cloud-clearing procedure at the National Centers for Environmental Prediction (NCEP) rejects a significant amount of radiance data in the area of a tropical storm affected by clouds and precipitation, thus eliminating crucial information about the storm. [The Advanced Microwave Sounding Unit (AMSU-B) radiances are plotted for Tropical Storm Erin for the period 1500–1800 UTC 18 August 2007.]

Since the launch of the Tropical Rainfall Measuring Mission (TRMM), the first satellite observatory specially designed to observe precipitation, significant efforts have been made to overcome the difficulties in assimilating precipitation data. Several research and operational efforts have been undertaken and produced successful results, thus ensuring that assimilation of cloudy radiances and precipitation sensitive satellite retrievals brings a value to both research and operations. For example, the National Aeronautics and Space Administration (NASA) Goddard Space Flight Center (GSFC) has produced TRMM global precipitation reanalyses using a weak-constraint variational approach for assimilating rain retrievals from microwave sensors, with evident positive data impact to have improved the accuracy of global precipitation estimates (Hou and Zhang 2007). NCEP has introduced rain retrievals into the operational global data assimilation system (e.g., Treadon et al. 2002). Other major meteorological centers, such as the Met Office, the Japan Meteorological Administration (JMA), and the European Centre for Medium-Range Weather Forecasts (ECMWF) have also been assimilating precipitation observations, precipitation-affected microwave radiances, and/or radar reflectivities (Macpherson 2001; Tsuyuki et al. 2002; Bauer et al. 2006a,b).

The above-mentioned and similar assimilation systems, even though advanced and resulting in significant improvements in precipitation analyses and forecasts, mostly focus on a global model resolution with parameterized physics schemes. In assimilating precipitation-affected radiances, precipitation and clouds can only be resolved at the global model grid resolution at 25 km or coarser, while a satellite instrument often observes inhomogeneous precipitation and clouds in its field of view (FOV). The relatively coarse temporal resolution in global models makes it necessary to assume that precipitation falls to the surface within one model time step, which results in additional parameterizations and assumptions to be made to meet the requirements of the rain-affected radiance calculation. Another difficult problem is that variational methods require inclusion of the nonlinear and discontinuous cloud and precipitation processes in the tangent linear model and its adjoint. When the complexity of moist physics increases, more substantial development work and simplifications have to be made to satisfy the linearization and minimization process (Lopez 2007). In operational variational data assimilation systems, some pragmatic approaches are taken to mitigate the difficulties. For example, Bauer et al. (2006a,b) introduced a one-dimensional variational (1D-Var) + four-dimensional variational (4D-Var) algorithm for the assimilation of precipitation-affected microwave radiances. The two-step approach, where satellite radiances are assimilated by the nonlinear 1D-Var step to produce increments of total column water vapor, and then these increments are assimilated by the linear (so-called incremental) 4D-Var step, has proven better in handling nonlinearities than the incremental 4D-Var approach alone. In Vukicevic et al. (2004, 2006), a different approach was taken to use a full blown 4D-Var with nonlinear updates of model-state variables during minimization and to assimilate the Geostationary Operational Environmental Satellite (GOES) imager brightness temperatures into a cloud-resolving model.

Advancements have been happening in the last decade in computer power, numerical modeling, physical retrieving techniques, and data assimilation methods, which have contributed to the improved utilization of precipitation-affected radiance observations, particularly for scientific applications that require high resolutions at cloud-resolving scales. For example, NASA Goddard cumulus ensemble (GCE) model runs in a 3D configuration

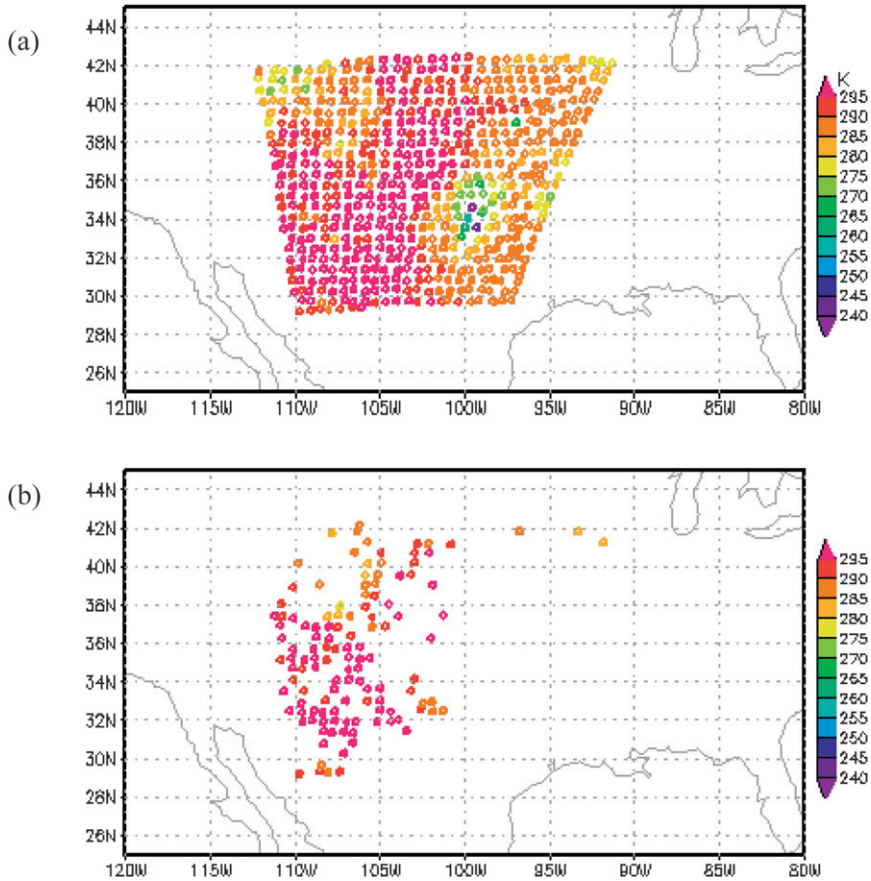

FIG. 1. Distribution of AMSU-B radiance data from the NCEP operational datastream: (a) all observations and (b) accepted observations after cloud clearing. Data are collected during the period 1500–1800 UTC 18 Aug 2007.

at the spatial resolution of 1 km or less, explicitly resolve clouds and associated precipitating processes. This has resulted in more detailed and improved simulations of cloud microphysical processes in comparison with single-column parameterized models that are commonly used at global model scales (Tao 2003). Cloud-resolving models (CRMs) have also played important roles in physical retrievals for precipitation and latent heating. For instance, in the physical retrieval systems of TRMM Microwave Imager (TMI) and the Advanced Microwave Scanning Radiometer for Earth Observing System (EOS) (AMSR-E), high-resolution hydrometeor distributions simulated by cloud-resolving models have been utilized to establish a database of profiles and corresponding simulated brightness temperatures for Bayesian inversion (Kummerow et al. 2001; Wilheit et al. 2003; Olson et al. 2006). Although there are many uncertainties on the accuracies and realistic depictions of hydrometeor variables in CRMs [e.g., Redelsperger et al. (2000) showed the large discrepancy of hydrometeor modeling among established cloud-resolving models with explicit microphysics], many ongoing studies and researches have been dedicated to evaluate and improve the microphysical schemes using a wide range of observations from field campaign data to high-resolution satellite observations (Zhou et al. 2007; Eito and Aonashi 2009; Matsui et al. 2009). These advances in cloud-resolving modeling are of importance for assimilation of precipitation-affected satellite radiances and radar reflectivity observations at cloud-resolving scales. Using models at cloud-resolving resolution in data assimilation provides a means to overcome the existing incompatibility between what coarse-resolution model physical parameterizations could resolve and what spaceborne instruments observe in reality; and it is essential for a data assimilation system to be applied to downscaling satellite precipitation observations for scientific applications in hydrological forecasts and regional climate studies.

Novel ensemble-based data assimilation methods hold the potential to overcome some of the difficulties of the variational methods in including cloud and precipitation data. The ensemble methods do not require tangent

linear models and adjoints of microphysics and radiance transfers. Instead, full nonlinear microphysics and radiance transfer schemes can be directly incorporated into assimilation procedures without explicit linearization or simplification. Tong and Xue (2005) applied an ensemble Kalman filter to the assimilation of Doppler radar data as an alternative to a variational approach. To investigate the ensemble representation of precipitation observation operators, an ensemble smoother was developed and assimilated rain retrievals from multiple microwave instruments into the Goddard GEOS-5 general circulation model (Zhang et al. 2008). At mesoscales, a recent study by Zupanski et al. (2010) applied an ensemble filter to assimilate synthetic cloudy IR radiances from the next-generation series of GOES-R Advanced Baseline Imager (ABI) instruments. The study also demonstrated that the forecast error covariance, updated by ensemble forecasts, is reflecting the occurring storm environment, which allows for maximizing information extracted from observations in the storm areas. The potential of these methods to further improve the analysis and the forecast of clouds and precipitation is also evident from Liu et al. (2008), Meng and Zhang (2008), Whitaker et al. (2008), and Aksoy et al. (2009). These pioneering efforts indicated that ensemble data assimilation methods offer a new path to an effective assimilation of precipitation-sensitive radiances at cloud-resolving scales. However, further exploring and evaluating of these methods is necessary, especially in evaluating their potential benefits for the future precipitation measurement missions, such as the Global Precipitation Measurement (GPM) mission.

The research presented in this manuscript was largely motivated by the scientific goals of the GPM mission. The GPM is an upcoming satellite mission, lead by NASA and the Japan Aerospace Exploration Agency (JAXA). It is composed of one core satellite and several constellation satellites, with dual-frequency precipitation radar (DPR) and a suite of microwave radiometers. GPM will systematically observe global precipitation systems with more frequent temporal and wider spatial data coverage than ever before. The observations obtained by GPM will provide valuable information about horizontal and vertical structures of precipitation, its macro- and microphysical nature, and its associated latent heating. A better understanding of the precipitation processes and their interconnections with dynamics and the water–energy cycle can push forward the current capabilities in weather, climate, and hydrological predictions. One of the most challenging scientific objectives of this mission is to optimally extract information from the available satellite observations and convert it into quantifiable improvements in forecast and analysis at multiple scales, ranging from global to cloud-resolving. NASA/GSFC and Colorado State University (CSU) joined forces to develop a prototype ensemble data assimilation system with a cloud-resolving model for assimilation and downscaling of precipitation information from GPM observations. The concept of the prototype system follows the special requirements for a high spatial and temporal resolution dynamically downscaled precipitation analysis: it utilizes a variety of observations from an operational datastream, a radiance transfer model to simulate precipitation-affected radiance, a high-resolution regional forecasting model with cloud-resolving microphysics, and an ensemble assimilation methodology. In this manuscript, we present the design of a prototype of the Weather Research and Forecasting (WRF)-based Ensemble Data Assimilation System (WRF-EDAS) and discuss results from a case study of assimilation experiments using NCEP operational datastream and AMSR-E radiance observations in cloudy and precipitating regions.

The manuscript is organized as follows. The system design is explained in section 2, the experiments of the case study are presented and discussed in section 3, and conclusions and future research directions are outlined in section 4.

2. System design

WRF-EDAS, a prototype ensemble data assimilation system using a cloud-resolving WRF model is developed jointly by NASA GSFC and CSU. The system is designed to assimilate precipitation-affected radiances from GPM observations as they become available. WRF-EDAS consists of the following components: (i) the Advanced Research WRF model (ARW-WRF; Skamarock et al. 2005), with NASA Goddard cloud microphysics and radiation schemes (GCE; Tao 2003); (ii) precipitation-affected radiance transfer models from NASA Goddard Satellite Data Simulation Unit (SDSU; Matsui et al. 2008); (iii) conventional and clear-sky radiance forward operators from the National Oceanic and Atmospheric Administration (NOAA)/NCEP's gridpoint statistical interpolation (GSI; Wu et al. 2002); and (iv) the maximum likelihood ensemble filter (MLEF; Zupanski 2005). The system configuration involving the above components is shown in a schematic chart in Fig. 2.

a. The forecast model and the control variables

The WRF model is configured to run in a regional domain with options to add nested inner domains with finer resolutions. The regional forecast runs use lateral boundary conditions from global forecast systems such as the NCEP Global Forecast System (GFS). The large-scale forcing is applied at the outer domain boundaries.

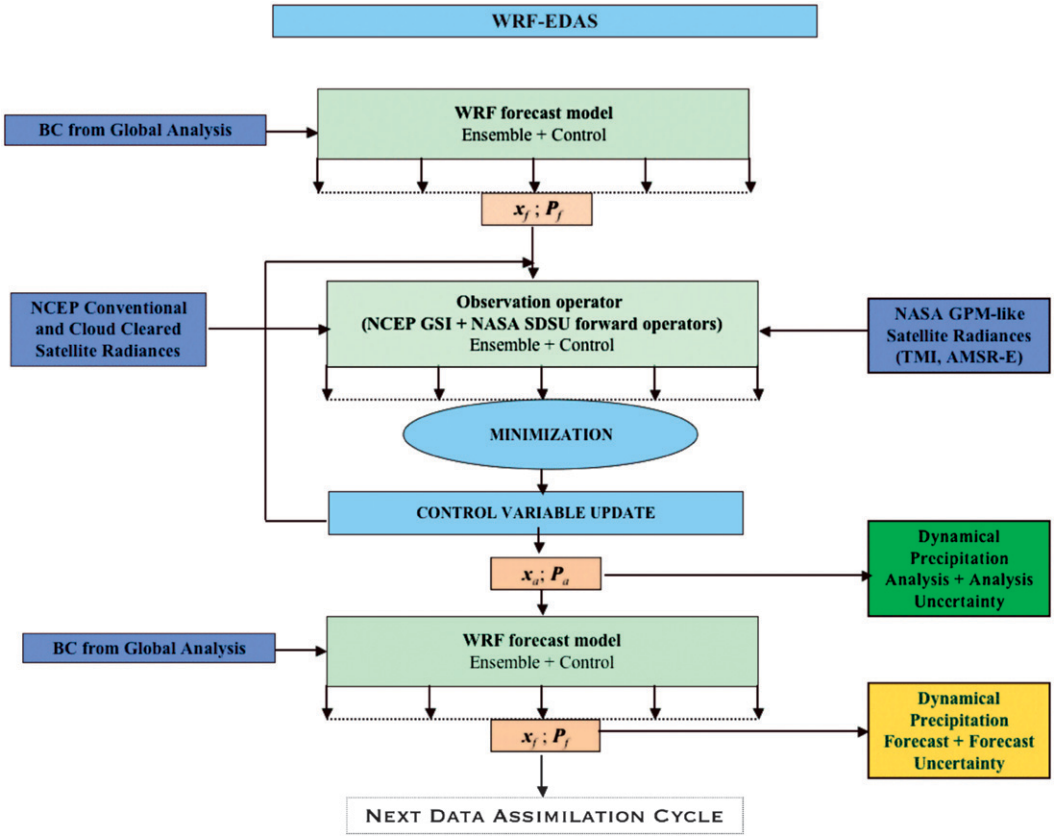

FIG. 2. Flowchart of WRF-EDAS.

In a nested domain run, the inner-domain boundary conditions are provided through the interaction with the outer domain. The cloud-resolving microphysics from GCE model (Tao 2003) is chosen particularly for high-resolution forecasts, for instance, in the inner domains of model grid size at 3 km or less. The cloud dynamics and the evolution of hydrometeor distributions in the atmosphere are explicitly resolved.

The control variables for the data assimilation are chosen from the WRF model prognostic variables consisting of u- and v-wind components, temperature, perturbation pressure, mixing ratios for water vapor, and the hydrometeor mixing ratios of cloud water, rain, ice, snow, and graupel. The configuration of control variables is designed to be flexible to include all or part of the prognostic variables listed above. Since the hydrometeors are directly related to the cloud and precipitation, these variables are included in the control vectors to explore the data impact on the analysis and forecasts, especially in the assimilation of precipitation observations. Since very little is known about the forecast error characteristics of the prognostic hydrometeor variables, we hope that ensemble forecasts and available observations will offer us an opportunity to examine the error distribution and evolution in the context of ensemble data assimilation with the chosen cloud-resolving model. The inclusion of the five hydrometeor types in the control variables also allows us to investigate their sensitivities corresponding to different microwave instrument channels under different surface conditions, so that statistics can be collected to guide the further development.

b. *The observations and forward operators*

To use the NOAA/NCEP operational datastream, the observation operators from NCEP GSI system are incorporated in WRF-EDAS. The forward operators for conventional data and clear-sky satellite radiances are adopted along with the operational observation error specifications, quality control, and bias correction procedures for these data types. During the data assimilation cycling, the large-scale forcing for forecasts is provided only at the domain boundaries. Use of these operational data is essential to provide information on the dynamical forcing in domain interiors. At the current prototype development stage, these data types include in situ conventional data and clear-sky satellite radiances

from selected channels of AMSU-A, AMSU-B, and the High Resolution Infrared Radiation Sounder (HIRS).

Observations from AMSR-E and TMI are the first set of precipitation-affected radiances to be used in the prototype system. The observation operators for the precipitation data are constructed from the CRM outputs and the radiative transfer models of NASA SDSU. The passive microwave simulator takes the background information from model forecasts including atmospheric variables and hydrometeors. A delta–Eddington two-stream radiative transfer with slant view (Olson and Kummerow 1996) calculates the brightness temperatures at the given model resolution. The simulated brightness temperatures are then convolved within the FOV of the specified sensor through a Gaussian beam pattern. For instance, to compare with an observation in a FOV of 14 km by 8 km (AMSR-E 36.5 GHz), 112 simulated brightness temperatures at a model resolution of 1-km grid size are convolved to produce the first guess of brightness temperature.

One big concern in precipitation-affected radiance assimilation is biases in simulated brightness temperatures, likely caused by biases in the model-predicted hydrometeors and some surface conditions particularly overland. A bias correction will be essential to ensure the quality of analysis. Previous studies on the CRM simulations using independent observations from field campaign data and satellite/radar observations provide valuable information about the biases. For example, Matsui et al. (2009) used collocated observations from TMI and precipitation radar (PR) to statistically evaluate the biases in the CRM-simulated frozen condensates and the formulation of the deep convection clouds. The development of a bias correction scheme is planned to focus on the CRM-predicted hydrometeor distributions and will use information from available observations to derive a parameterized bias correction algorithm, and the correction parameters will be estimated and updated along the assimilation cycling.

c. *The ensemble data assimilation algorithm*

The MLEF, with its iterative, nondifferentiable minimization (Zupanski et al. 2008), is an important component of WRF-EDAS. It provides a means to assimilate precipitation sensitive observations through the use of nonlinear and discontinuous observation operators without a need for an explicit tangent linear model and adjoint for precipitation observations. For instance, the innovations of precipitation-affected brightness temperatures are calculated using full model physics and radiative transfer. The ensemble innovation covariance is used to project information between control variable space and observation space. The algorithm details of MLEF are given in the appendix. Being an ensemble-based method, the MLEF uses ensemble-based, flow-dependent forecast error covariances and updates them in each data assimilation cycle. The flow-dependent forecast error covariance involves cross correlations between the cloud microphysical variables and model dynamical variables and, if described realistically, would ensure a dynamically balanced precipitation analysis. As a consequence, the impact of precipitation assimilation would have a better chance to extend into the forecast, since it was ''remembered'' by the model dynamics.

The error covariance based on ensemble forecasts can be noisy because of a relatively small ensemble size. Localization or other filtering schemes can be applied to control or filter the noise. The error covariance localization algorithm employed in the MLEF is the weight-interpolation method of Yang et al. (2009). The weight-interpolation method incorporates an interpolation in ensemble space, rather than in physical space. Since the computationally expensive matrix–matrix calculations before interpolation are done on a coarse grid, the method of Yang et al. (2009) is also computationally more efficient than the original localization method of Hunt et al. (2007) and Miyoshi and Yamane (2007). In application with the MLEF, the only difference from the method described in Yang et al. (2009) is that the control variable in the ensemble space is interpolated, rather than the weight coefficients. This is due to the algorithmic design of the MLEF as an iterative minimization.

The MLEF employs a nonlinear and nondifferentiable minimization algorithm described in Zupanski et al. (2008—algorithm 1). The algorithm is roughly based on a nonlinear conjugate gradient algorithm (e.g., Luenberger 1984); however, it is defined using a generalized gradient and Hessian to avoid potential problems with nondifferentiable functions. Different from previous MLEF applications, the line-search procedure in iterative minimization is performed locally, rather than globally, implying a minimization of local cost functions. This allows better fit to observations and eventually improves the filter performance.

3. Experiments of Tropical Storm Erin (2007)

The prototype system of the WRF-EDAS is built with a high-resolution WRF model, a set of observation operators for in situ and remote-sensed observations, and an analysis scheme to handle nonlinearity and background error covariance localization. To test and evaluate the system, we carried out data assimilation experiments for a case of Tropical Storm Erin, which was formed in the Gulf of Mexico in August 2007. This tropical storm was especially difficult to predict because it went through

an overland reintensification over Oklahoma from 0000 through 1500 UTC 19 August 2007, producing hurricane strength winds and heavy precipitation (e.g., Knabb 2008; Arndt et al. 2009). We focus on this period of the storm reintensification in data assimilation experiments of this study in two sets of experiments: 1) one to evaluate the performance of WRF-EDAS in assimilation of the NCEP operational datastream (including conventional and cloud-cleared satellite radiance data) using results from NCEP WRF-GSI system as a benchmark, and 2) one to investigate the viability of direct radiance assimilation of precipitation-affected AMSR-E observations within the WRF-EDAS.

In this experimental system setting, the WRF model employs a parent domain and a nest, with horizontal grid spacing of 9 and 3 km, respectively. The parent domain includes $241 \times 160 \times 31$ grid points, and the nest includes $385 \times 268 \times 31$ grid points. The regional boundary conditions were constructed from the NCEP GFS analyses and were not perturbed by the ensembles. The control variables consist of u- and v-wind components, temperature, perturbation pressure, mixing ratio for water vapor, and five different hydrometeors (mixing ratios for cloud water, rain, ice, snow, and graupel). The data assimilation is performed every 3 h, for both grids, using available NCEP conventional data, clear-sky satellite radiances from selected channels, and precipitation-affected radiances from AMSR-E. The ensemble size of 32 members is used, and a covariance localization scheme is applied to improve the representation of the degrees of freedom (DOF) in the system.

a. Assimilation of conventional and clear-sky radiance observations

We performed data assimilation experiments for the period from 1500 UTC 18 August 2007 through 0600 UTC 19 August 2007, assimilating conventional and satellite observations from the NCEP observational datastream every 3 h. Conventional observations, available in the model domain, include Surface Synoptic Observations (SYNOP), ship-collected water surface data, radiosonde, pilot, wind profiler, velocity–azimuth display (VAD) winds, satellite cloud-drift winds, aircraft, and the GPS-integrated precipitable water data. Satellite observations, available in the model domain, include clear-sky AMSU-A, AMSU-B, HIRS, Microwave Humidity Sounder (MHS), and Atmospheric Infrared Sounder (AIRS) radiances. The same observations are assimilated in both WRF-EDAS and WRF-GSI. We also use the same observation errors in both systems, except for the fact the observation errors were multiplied by the scaling factor 1.25 in WRF-EDAS. The scaling factor accounts for differences between the two systems, such as differences between the forecast error covariances, and it was determined to approximately satisfy the expected chi-square innovation statistics, assuming Gaussian error distribution (e.g., Menard et al. 2000; Zupanski 2005). In this set of experiments, the WRF model was run using only the 9-km-resolution parent domain in both WRF-EDAS and WRF-GSI.

Figures 3a and 3b show the first-guess (3 h) forecasts of sea level pressure valid at 0600 UTC 19 August 2007: the GSI results are given in Fig. 3a and the WRF-EDAS in Fig. 3b. The NOAA surface weather map is shown in Fig. 3c for the reference of observed storm location, valid at the same time. The time of 0600 UTC is the moment when the cyclone reached the minimum surface level pressure of 995 hPa at the storm center (according to the Erin best-track report of Knabb 2008). As shown in the figure, WRF-EDAS produced a deeper cyclone (1003 hPa), with more closed isolines, than that from GSI (1009 hPa). The cyclone was still not deep enough in both experiments to reach the observed minimum of 995 hPa.

In Fig. 4, we present the first-guess forecast of surface wind for the two experiments, valid at the same time as in Fig. 3 (0600 UTC). It is evident that WRF-EDAS produced a stronger and more organized cyclone compared to that from GSI, with the maximum wind intensity of 16 m s^{-1} (versus 12.5 m s^{-1} in the GSI). Though this is still an underestimation compared to the observed wind intensity of 25.72 m s^{-1} (Knabb 2008), the relatively improved representation of the storm intensity and structure demonstrated the capability of WRF-EDAS to extract information from a common set of observations effectively.

The short-term 3-h forecasts from the two data assimilation systems over seven consecutive data assimilation cycles, covering the period from 1500 UTC 18 August through 0900 UTC 19 August 2007, are summarized in Figs. 5 and 6. The root-mean-square (RMS) errors of the 3-h forecasts (forecast verified against in situ data) are shown in Fig. 5. The forecast errors of WRF-EDAS are smaller than that of GSI for u- and v-wind components and temperature at most levels. The errors are comparable for the humidity, with slight degradation in the WRF-EDAS at lower levels. The comparison of the forecast departures indicate that the prototype WRF-EDAS is stable and maintains a reasonably accurate dynamic forcing in the domain at a similar level as that of the established system GSI, when the same high-resolution model and the same set of observations are used. To verify the surface rain from the WRF-EDAS 3-h forecasts in comparison with that of GSI, observations from NCEP stage IV national mosaic are used. Figure 6 shows the GSI forecast (Fig. 6a), the WRF-EDAS forecast (Fig. 6b), and the NCEP stage IV observations (Fig. 6c) of total surface precipitation, accumulated over the same data assimilation cycles as in Fig. 5. As the

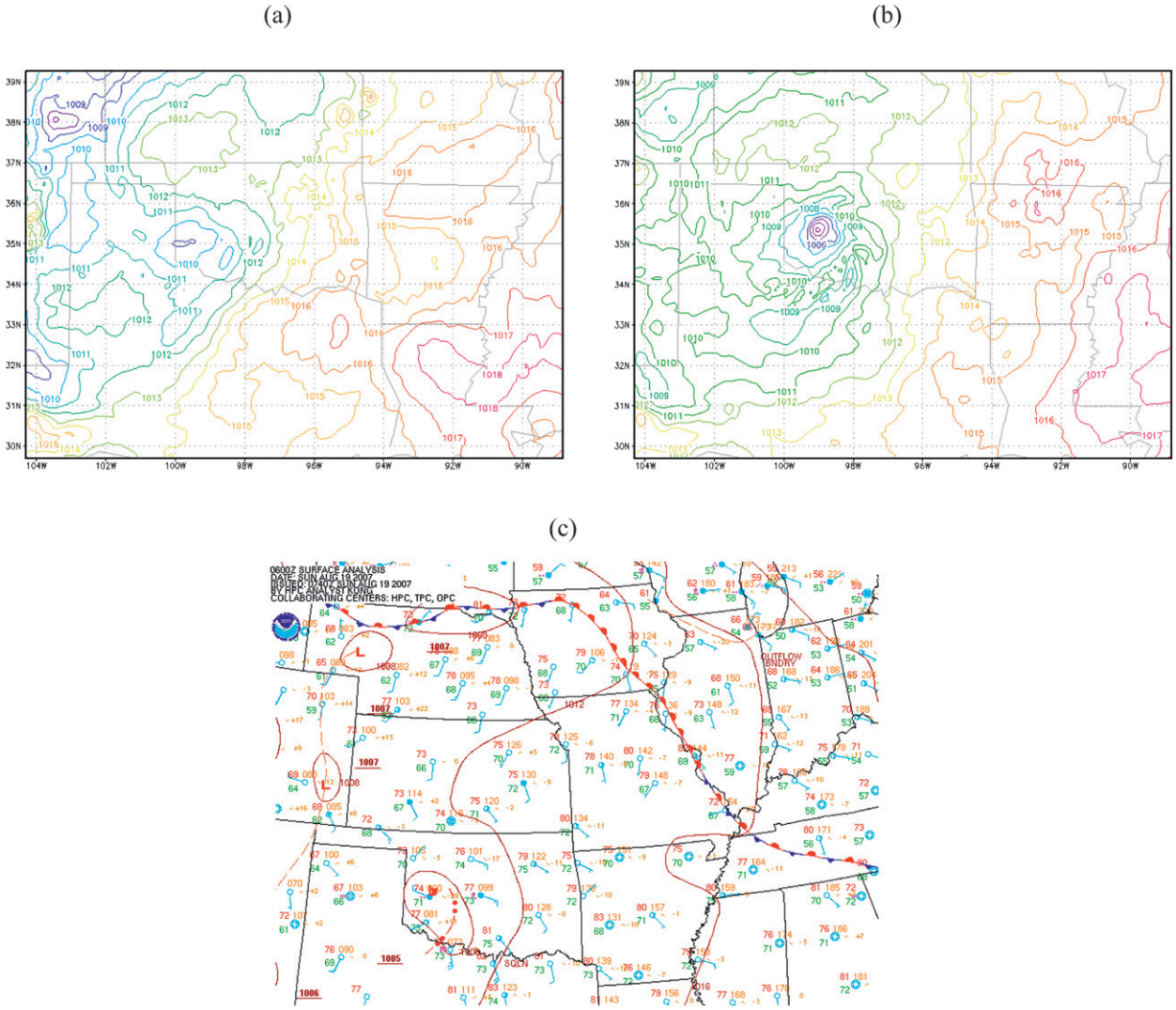

FIG. 3. Sea level pressure valid at 0600 UTC 19 Aug 2007. First-guess (3 h) forecasts are shown for (a) GSI and (b) WRF-EDAS. (c) The National Weather Service surface map for location reference. Results from the 9-km WRF grid are shown, presenting only the area of interest (centered on Oklahoma).

observations indicate, the maximum-accumulated precipitation of 300 mm occurred in south-central Oklahoma. This maximum is missing in the GSI-based forecast (it is too weak and shifted too far toward central Texas). The precipitation pattern is in better agreement with the observations in the WRF-EDAS forecast with the precipitation maximum of the same magnitude as observed. Note, however, that the precipitation maximum is shifted slightly toward the southeast.

The results obtained from these experiments provided reasonable confidence to the performance of the WRF-EDAS using WRF-GSI as a benchmark, thus ensuring a good background for data assimilation experiments when precipitation-affected radiances are added.

b. Assimilation of precipitation-affected AMSR-E radiances

In the domain of Erin reintensification over Oklahoma, one swath of AMSR-E observations is available at 0900 UTC 19 August 2007. AMSR-E is a 12-channel, 6-frequency passive microwave radiometer system. It measures horizontally and vertically polarized brightness temperatures at 6.9, 10.7, 18.7, 23.8, 36.5, and 89.0 GHz. A preassimilation-check procedure is carried out to all channels of brightness temperatures from AMSR-E level 2A swath data for the period covered by the experiments. Using 9- and 3-km-resolution WRF forecasts and the radiative transfer model, brightness temperatures for

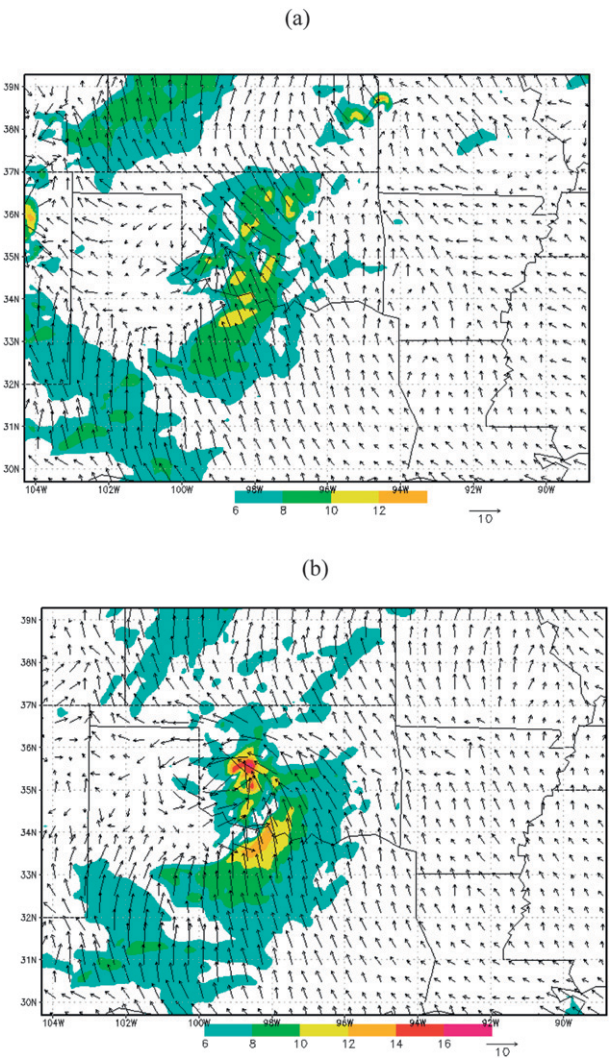

FIG. 4. Surface wind (at 10 m above ground), valid at 0600 UTC 19 Aug 2007, obtained as 3-h forecasts from (a) GSI and the (b) WRF-EDAS. Results from the larger model domain with 9-km grid spacing are shown, presenting only the area of interest.

different channels are simulated and compared with the observations. The observation error standard deviation is empirically prescribed taking into account the instrument errors and forward model errors. In this experiment, the brightness temperature observation error standard deviations are empirically set to 18 K for 37 and 89 GHz, as well as 20 K for all other channels. An ad hoc quality control is applied to screen out the extreme outliers; for example, the observations at 89 GHz exceeding the prescribed threshold 300 K, or observations where the departure amplitudes are as big as the signal itself. The observations in the swath are not thinned, and a nearest-point scheme is used to determine the model grid point at the center of the FOV that matches the observation location. Though biases are observed from the collection of departures; for instance, a 10-K bias in the 89-GHz channel based on 300 departures collected in the raining area, the number of observations used in the check procedure is not sufficient to formulate a reliable bias correction. An online bias correction is yet to be developed and implemented. However, because the experiment is set overland, bias from using different microwave land surface emissivity schemes is examined. For instance, simulated brightness temperatures at 24 GHz using the Goddard land emissivity scheme has a 20-K bias compared with observations under no-rain condition. The higher-frequency channel of 89 GHz is much less affected. The bias under the same condition is much smaller when the National Environmental Satellite, Data, and Information Service (NESDIS) land emissivity scheme is used, whereas other comparison studies indicate that biases from different land emissivity schemes vary from regions and seasons. Based on the limited data statistics we have had so far, the NESDIS emissivity scheme is chosen in the microwave radiance transfer for this experiment. In this case study, where the land emissivity is relatively homogenous, a bias of 5 K is removed from the departures of 19- and 24-GHz channels at the analysis time.

The ensemble WRF forecasts are configured with the parent domain (9-km horizontal resolution) and the nest (3-km resolution) where the storm is present and is covered by the AMSR-E data swath. In the nest domain, the microphysics is used to explicitly resolve the cloud and precipitation processes. The perturbations to the parent domain model state are applied as that to single-domain forecasts, and this also provides the initial perturbations to each ensemble member of the nest domain.

Figure 7 illustrates how the assimilation of precipitation-affected radiance observations influences the analysis in observation space (brightness temperatures). The analysis of brightness temperature is obtained by applying the radiance transfer operator to the analysis of model-state variables (wind, temperature, pressure, humidity, and five hydrometeors). We show the 89-GHz *V* channel as an example of channels with strong signals, but the results from other rain-sensitive channels such as 23.8 and 36.5 GHz are qualitatively similar. We keep all channels for the generality of the observation datastream development and for applications in different regions (overland or overwater). In this case study, the lowest-frequency channels of AMSR-E have very little sensitivity to hydrometeors in the assimilation procedure. The precipitation signals in the midrange-frequency channels are relatively weak overland mainly because of the high and variable emissivity from the background. However, these channels do exhibit some sensitivity to the distribution

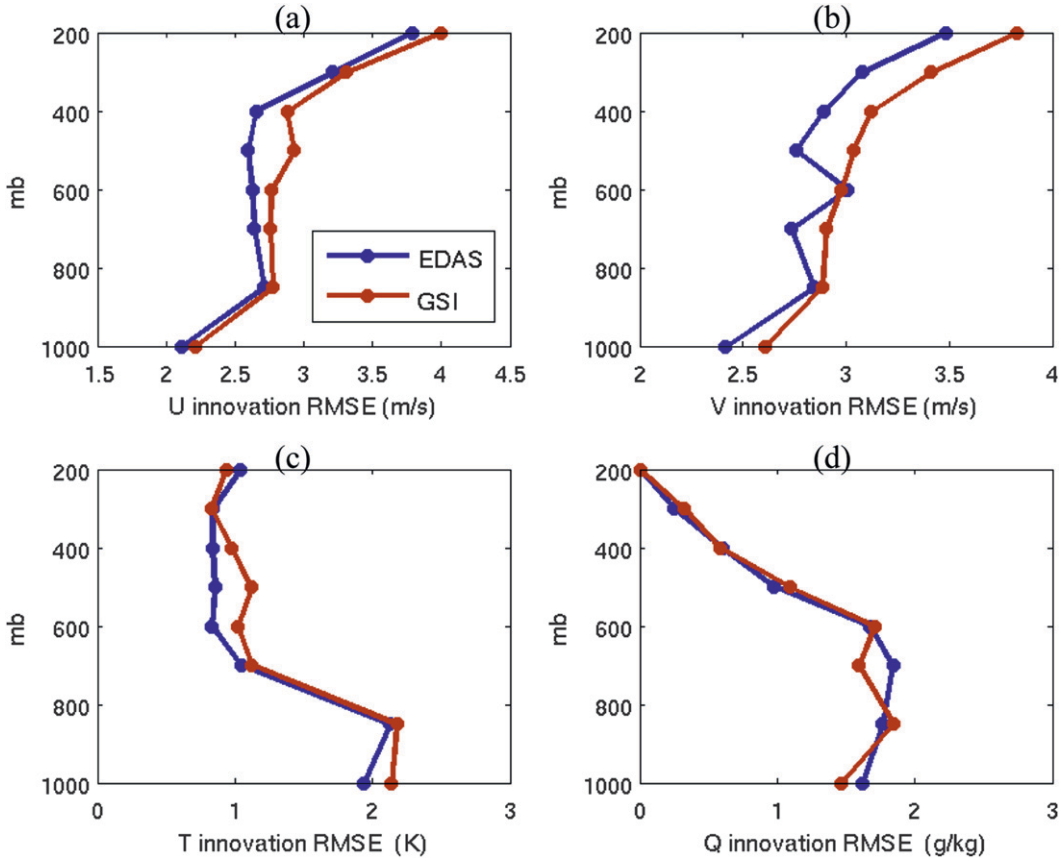

FIG. 5. Vertical profiles of the first-guess errors from the WRF-EDAS and GSI data assimilation systems: RMS errors for the (a) u-wind component, (b) v-wind component, (c) temperature, and (d) humidity. The errors are calculated with respect to the NCEP conventional observations over seven data assimilation cycles (covering the period from 1500 UTC 18 Aug 2007 to 0900 UTC 19 Aug 2007).

of hydrometeors in the atmosphere below the freezing level, particularly in this case study where heavy rainfall is observed. As seen in Fig. 7a, there is a strong signal in the observations indicating cold brightness temperatures in the storm area, associated with clouds and precipitation. The first-guess departure field, shown in Fig. 7b, indicates there is significant discrepancy in terms of brightness temperature depression in the storm area. There is also a dipole pattern (red–blue colors) suggesting a mismatched first-guess precipitation pattern with respect to the observations. These errors are considerably reduced in the analysis in Fig. 7c: the maximum errors are now reduced by 30%, and the dipole pattern is less pronounced.

When the direct radiance assimilation reduced errors in the observation space of the brightness temperature, what is the impact to the hydrometeor distributions? In Fig. 8, we show cross sections of brightness temperature and increments of two hydrometeors (rain and snow) taken through the storm along the longitude of −98.4°E. By examining the upper panel (Fig. 8a) one can notice that the analysis is closer to the observations than the first guess, matching the two minima better. Looking at the lower panel (Fig. 8b) we can see how the hydrometeor fields of rain and snow have responded to fit the observations better. There is an increase (warm colors) in rain, at the lower levels, and in snow, at the upper levels, toward a better fit of the brightness temperature minima. The negative (blue colors) increments represent reduced precipitation. There is also a location shift in the precipitation pattern (corresponding to a correction to the pattern mismatch in Fig. 7).

Figure 9 shows the results from the nested domain (with 3-km grid spacing). The higher resolution and microphysics allow for a more detailed model simulation of the precipitation system and finer structures in simulated brightness temperatures. As seen in the upper panels, the precipitation intensity is increased, represented by the lower brightness temperatures (deeper blue color) in the analysis (right) with respect to the first guess (left), in the area of the storm. Comparing the two scatter diagrams, it is evident that the discrepancy between observed and model-simulated brightness temperatures is

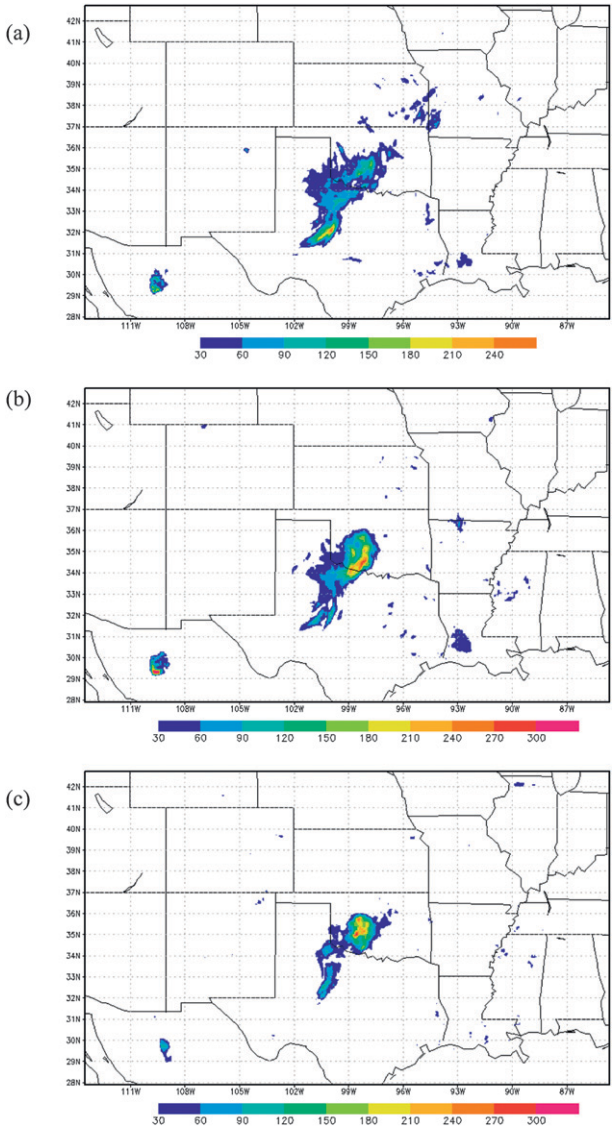

FIG. 6. Total (convective + stratiform) precipitation (mm), accumulated over the period from 1500 UTC 18 Aug 2007 to 0900 UTC 19 Aug 2007 (from seven consecutive data assimilation cycles) from (a) GSI and (b) WRF-EDAS. (c) The observed values (from the NCEP stage IV national mosaic). The grid spacing of the observations is 4 km.

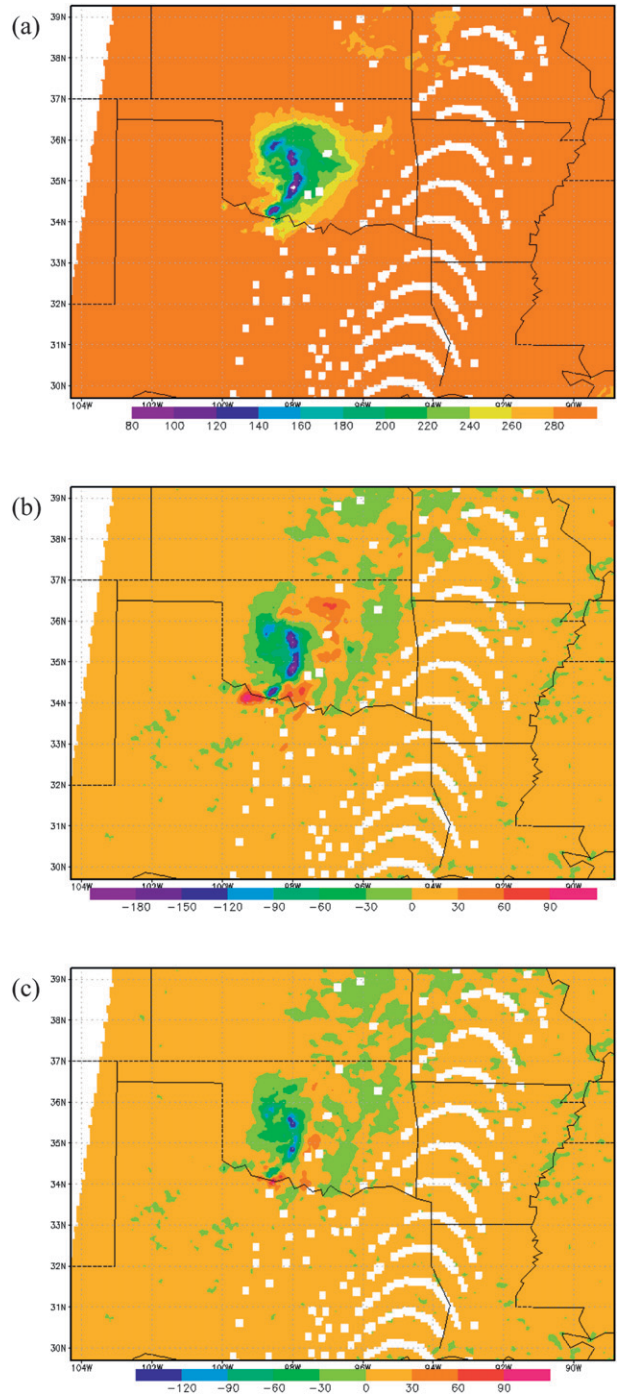

FIG. 7. AMSR-E brightness temperature of 89-GHz V (K) valid at 0900 UTC 19 Aug 2007 for the WRF-EDAS outer domain: (a) observed brightness temperature, (b) the observation minus forecast differences, and (c) the observation minus analysis differences.

reduced by assimilating AMSR-E data, especially in the precipitation sensitive range of brightness temperatures.

In addition to the analysis increments on cloud microphysical variables, assimilating AMSR-E brightness temperatures has an impact to other control variables as well. In ensemble data assimilation, such potential influence could be provided by the cross covariance in ensemble-estimated background error covariance, for instance, observations made to the variables of hydrometeors can potentially generate analysis increments on the variables of wind that are not observed at the time. An illustrative example is given in Fig. 10. Two ''data denial'' experiments for this particular analysis time (0900 UTC 19 August 2007) are shown here. The first-guess wind field is identical in both experiments shown

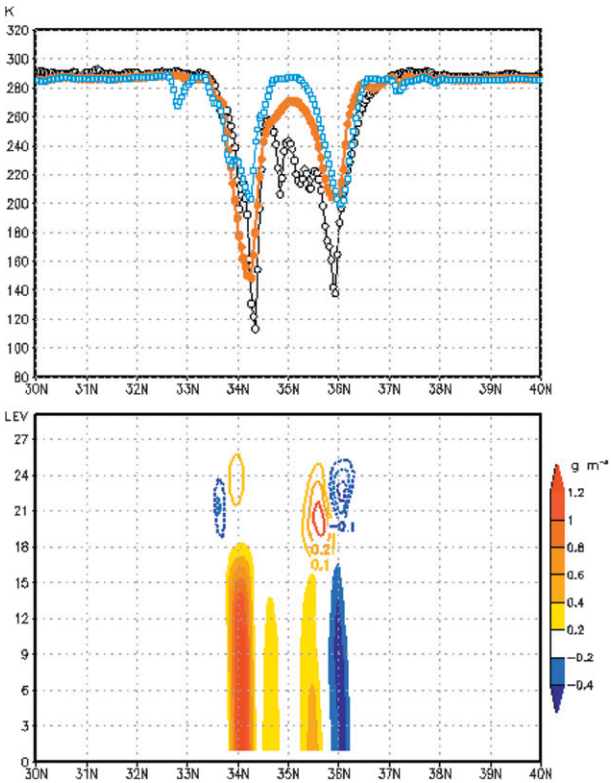

FIG. 8. Vertical cross section through the storm at longitude −98.4°E, valid at 0900 UTC 19 Aug 2007 for the WRF-EDAS outer domain: (top) the AMSR-E brightness temperature of 89-GHz V (K) for the observations (black), first guess (blue), and the analysis (orange) as a function of latitude, and (bottom) the analysis increments (i.e., differences between the analysis and the first guess) for mixing ratios of rain (shaded) and snow (contours; g kg^{-1}) as functions of latitude and vertical levels.

in Fig. 10a. The experiment ''NCEP data only'' uses operational observations on dynamic fields but does not use precipitation radiance data. In the opposite, experiment ''AMSR-E data only'' uses precipitation radiance only, not using any direct observations on dynamic fields. Comparing wind convergence and cyclonic circulation in the analysis increments at 700 hPa shown in Fig. 10b (AMSR-E data only) and Fig. 10c (NCEP data only), both sets of observations produce corrections to increase the storm strength around the storm center, even though the AMSR-E radiances are not directly observing wind field. This is a direct consequence of forecast error cross covariance between dynamical and cloud microphysical variables. These results demonstrate that the analysis increment, and consequently the cross covariance between wind and cloud microphysical variables, are flow-dependent and reflecting the up-to-date dynamical environment of the storm. Nevertheless, a stricter quantitative analysis, performed over a longer time period, is still needed for more general conclusions.

In this case study, the AMSR-E data is assimilated only at one analysis time simultaneously along with other observations (NCEP conventional and clear-sky satellite data). Constraint is implicitly applied by the cross correlations between different components in the control variable as described by the flow-dependent forecast error covariance. Whether the analysis solution is optimal and how it impacts precipitation forecasts depend on many factors in the assimilation procedure, such as realistic and well-tuned error statistics, unbiased model forecasts, and observations; and the ultimate validations need to be done with independent observations and statistical verifications in atmospheric states such as precipitation, moisture, temperature, and dynamical variables in longer periods and broader ranges of conditions. Nevertheless, within the limit of a case study, we will examine how the assimilation of precipitation radiance influences the short-term (3 h) forecasts, and hope the study will at least provide a starting point to explore the potential benefits and possible problems. Two sets of high-resolution forecasts (3-km grid) are issued from the analyses at 0900 UTC (with and without AMSR-E data). The accumulated surface rain forecasts are shown in Fig. 11. The difference between panels (a) and (b) shows that the assimilation of AMSR-E data induced excessive surface rain accumulation, comparing with the verification data given in panel (c). This indicates that the analysis corrections on the initial rainwater distribution at lower model levels may be too large in fitting with the very strong scattering observed by high-frequency channels, even though ice condensates above the freezing level are included in the control variables. It also highlights the importance of the bias correction as well as a rigorous quality control in using precipitation-affected radiances. In this assimilation experiment, the systematic errors are not yet estimated or corrected. The observation error specification is preliminarily based on a limited amount of observations. Some large radiance departures at higher-frequency channels on the order of 100 K are not excluded by the ad hoc data rejection scheme. Therefore, analysis increments are likely affected and biased by these big departures. Another factor is that the microphysics scheme is activated at this 3-km resolution in the inner domain, and the model physics responds to the analysis perturbations with stronger convection and higher rain efficiency, which produces sustained heavy rain.

The relationship between model-predicted surface rain accumulation and the analysis correction to the initial model-state variables is certainly not simple. The precipitation forecast skills depend on not only the quality of the analysis, but also how the model physics respond to analysis perturbations onto the distribution of rainwater, snow, ice, etc. and produce rainfall that reaches

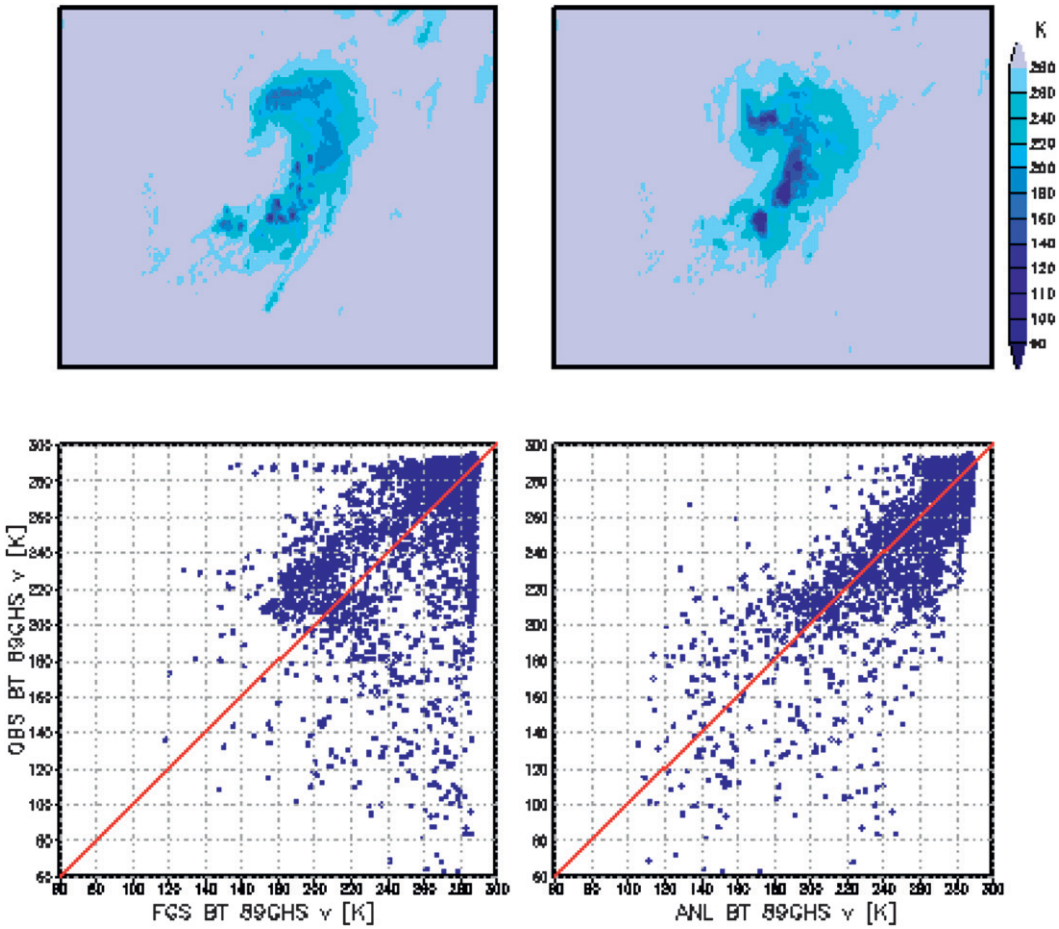

FIG. 9. AMSR-E brightness temperature of 89-GHz V (K) valid at 0900 UTC 19 Aug 2007 for the inner domain of the WRF (with 3-km grid spacing): the (top left) first guess and (top right) analysis, and (bottom) the scatter diagrams of (left) the observed vs first guess and (right) the observed vs analysis.

the surface. The Erin reintensification case study presented here has demonstrated that the assimilation of precipitation-affected radiances can profoundly influence the precipitation and other dynamical fields. It also highlights the important issues to be investigated that will lead to the further development of WRF-EDAS.

4. Conclusions and future work

A prototype WRF ensemble data assimilation system (WRF-EDAS) is developed as a test bed to explore a dynamic downscaling method using ensemble data assimilation techniques and cloud-resolving models. Experimental results are presented from a case study assimilating the NCEP operational datastream and precipitation-affected AMSR-E radiances. The prototype WRF-EDAS is designed for hydrological applications that require downscaled precipitation from the upcoming GPM satellite precipitation observations. The system is constructed with the components of a high-resolution ARW-WRF with NASA cloud microphysics and nesting capability, observation operators for conventional data and clear-sky satellite radiances derived from the NCEP GSI, observation operators for precipitation-affected satellite radiances derived from the NASA SDSU, and the ensemble data assimilation algorithm based on the maximum likelihood ensemble filter.

A case study on Tropical Storm Erin (2007) is presented to investigate the ability of the prototype of WRF-EDAS to ingest information from in situ and satellite observations including precipitation-affected radiance. The first set of experiments assimilates in situ data and clear-sky radiances from NCEP operational datastream, and the NCEP WRF-GSI analysis system is used as a benchmark. The short-term forecast, initiated using WRF-EDAS, predicted the tropical storm reintensification reasonably well in terms of both minimum surface pressure at the storm center and the maximum surface

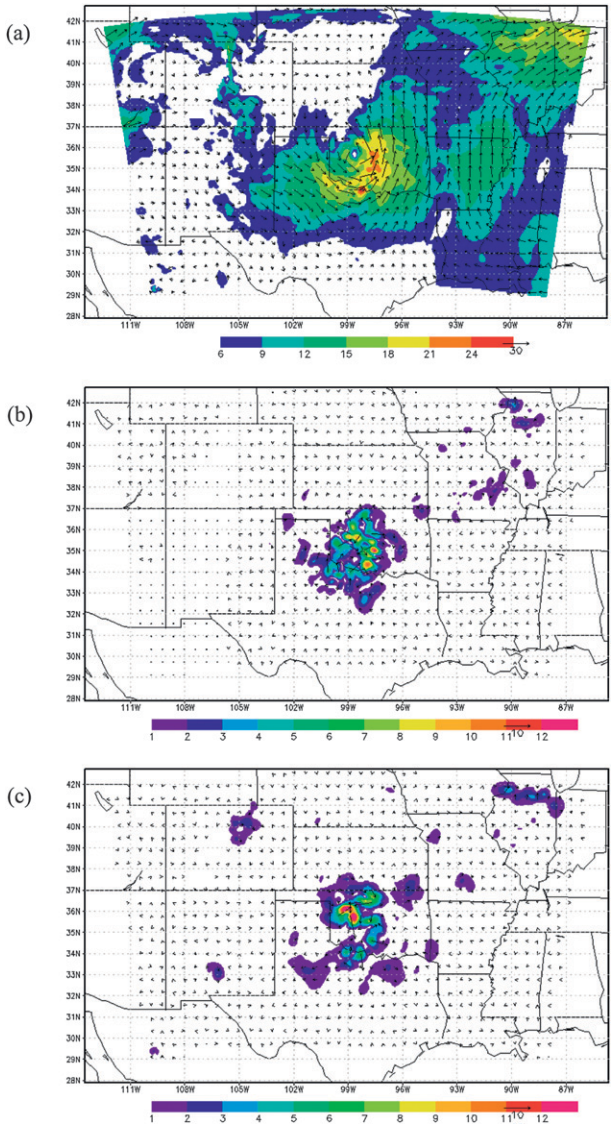

FIG. 10. Wind field at 700 hPa (m s^{-1}) valid at 0900 UTC 19 Aug 2007 for (a) the first-guess forecast, (b) WRF-EDAS analysis increments (analysis minus first-guess differences) using AMSR-E radiances only, and (c) analysis increments using NCEP data only (conventional data + clear-sky radiances). The colors indicate wind vector magnitude, and the arrows show both wind magnitude and direction.

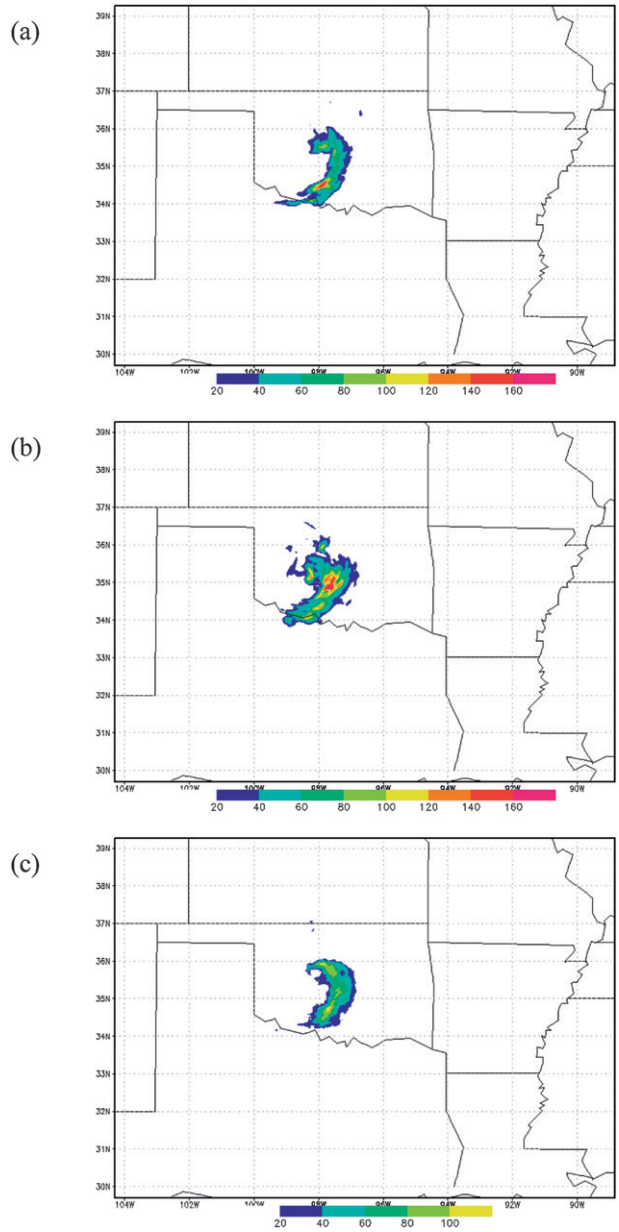

FIG. 11. Total (convective + stratiform) precipitation (mm) obtained as 3-h forecasts after data assimilation valid at 1200 UTC 19 Aug 2007 for (a) the forecast from the WRF-EDAS using NCEP data only, (b) the forecast from the WRF-EDAS using NCEP data and AMSR-E radiances, and (c) the observed precipitation (from the stage IV national mosaic). The forecast results are from the 3-km-resolution inner domain, and the verification data are at 4-km resolution.

wind intensity. The precipitation pattern of accumulated precipitation over several data assimilation cycles was in good agreement with the observed NCEP stage IV national mosaic precipitation data. Comparisons of the short-term forecast errors of WRF-EDAS and WRF-GSI, calculated as RMS errors with respect to the conventional observations, show that the forecasts produced by the WRF-EDAS system are comparable to or better than those obtained with the WRF-GSI analysis scheme using the same set of observations. The second set of experiments assimilates precipitation-affected radiances from AMSR-E available during the period of storm reintensification in the domain. The assimilation of AMSR-E radiances increases the precipitation intensity and corrects the precipitation spatial patterns in the storm region. The data denial experiment illustrates that the information

in the precipitation-affected radiances is extended into wind fields through the use of the flow-dependent forecast error cross covariance between wind and cloud microphysical variables. The influence of AMSR-E radiances to short-term precipitation forecasts is investigated by the twin forecasts issued from initial conditions with or without AMSR-E data assimilated. The quantitative verification of the forecasted accumulated precipitation amounts indicates that the analysis increments from AMSR-E data induce excessive surface rainfall in the forecast verified against the NCEP stage IV precipitation data. These results highlight the critical issues of bias correction and rigorous quality control for precipitation-affected radiances, and call for a better understanding of the microphysics behaviors in the data assimilation system.

The preliminary results from the case study provide a starting point to explore what aspects of the ensemble data assimilation system and the cloud-resolving model may influence the quality of analyses and forecasts and information on important issues to address in the future development of the system. Further development work will focus on the estimating of systematic and random errors in the simulation of brightness temperatures, assessing the background error covariance of hydrometeor variables from ensemble forecasts, evaluating model response of different hydrometeors to radiance assimilation, and validating assimilation results systematically using ground validation datasets and spaceborne observations.

While further work is needed to optimize the performance of the WRF-EDAS, this study establishes the viability of developing a cloud-scale ensemble data assimilation system that has the potential to provide a useful vehicle for downscaling satellite precipitation information to finer scales suitable for hydrological applications.

Acknowledgments. This research was supported by the GPM Flight Project at NASA Goddard Space Flight Center, and NASA Precipitation Measurement Mission (PMM) Science Program under Grant NNX07AD75G to Colorado State University. The authors of this manuscript would like to thank Toshi Takemura and William Olson for providing radiative transfer models, and W.-K. Tao and Roger Shi for providing Goddard microphysics schemes. The AMSR-E radiance data was provided by National Snow and Ice Data Center, and computations were carried out at NASA Advanced Supercomputing (NAS).

APPENDIX

MLEF Overview

In the MLEF, the optimal analysis is obtained by maximizing the posterior conditional probability density function (PDF). In practice, this is achieved by an iterative minimization of a cost function

$$\mathcal{J}(\mathbf{x}) = \frac{1}{2}(\mathbf{x}-\mathbf{x}^f)^{\mathrm{T}}\mathbf{P}_f^{-1}(\mathbf{x}-\mathbf{x}^f) + \frac{1}{2}[\mathbf{y}-\mathcal{H}(\mathbf{x})]^{\mathrm{T}}\mathbf{R}^{-1}[\mathbf{y}-\mathcal{H}(\mathbf{x})], \quad \text{(A1)}$$

where $\mathbf{R}$ is the observation error covariance, $\mathbf{P}_f$ is the forecast error covariance, $\mathbf{y}$ is the observation vector, $\mathbf{x}$ is the state vector, and $\mathcal{H}$ is a nonlinear observation operator. The superscript f refers to the first-guess forecast. The matrix $\mathbf{P}_f$ is defined in a subspace spanned by ensemble forecast increments as

$$\mathbf{P}_f^{1/2} = [\,\mathbf{p}_1^f \quad \mathbf{p}_2^f \quad \cdots \quad \mathbf{p}_{N_E}^f], \quad \text{where}$$
$$\mathbf{p}_i^f = \mathcal{M}(\mathbf{x}^a + \mathbf{p}_i^a) - \mathcal{M}(\mathbf{x}^a), \quad \text{(A2)}$$

$\mathcal{M}$ denotes the nonlinear forecast model, the superscript a refers to the analysis, and N_E is the number of ensembles. The vectors $\mathbf{p}_i^a$ and $\mathbf{p}_i^f$ represent the columns of the square-root analysis and forecast error covariances, respectively. If the state vector dimension is denoted N_S, then the square-root forecast error covariance is an $N_S \times N_E$ matrix.

A unique feature of the MLEF is an implicit Hessian preconditioning, achieved by the control variable transformation

$$\mathbf{x} - \mathbf{x}^f = \mathbf{G}\boldsymbol{\zeta}, \quad \text{where}$$
$$\mathbf{G} = \mathbf{P}_f^{1/2}\left\{\mathbf{I}_{N_E} + [\mathbf{Z}(\mathbf{x}^f)]^{\mathrm{T}}\mathbf{Z}(\mathbf{x}^f)\right\}^{-1/2}, \quad \text{(A3)}$$

$\mathbf{I}_{N_E}$ is an $N_E \times N_E$ identity matrix, $\boldsymbol{\zeta}$ is the control variable in ensemble space, and the matrix $\mathbf{Z}(\mathbf{x}^f)$ is the observation perturbation matrix defined at the first guess $\mathbf{x}^f$ as

$$\mathbf{Z}(\mathbf{x}^f) = [\mathbf{z}_1(\mathbf{x}^f) \quad \mathbf{z}_2(\mathbf{x}^f) \quad \cdot \quad \cdot \quad \mathbf{z}_{N_E}(\mathbf{x}^f)], \quad \text{where}$$
$$\mathbf{z}_i(\mathbf{x}^f) = \mathbf{R}^{-1/2}[\mathcal{H}(\mathbf{x}^f + \mathbf{p}_i^f) - \mathcal{H}(\mathbf{x}^f)]. \quad \text{(A4)}$$

We can also define the observation information matrix calculated at the first guess as matrix

$$\mathbf{C}(\mathbf{x}^f) = \mathbf{Z}(\mathbf{x}^f)^{\mathrm{T}}\mathbf{Z}(\mathbf{x}^f). \quad \text{(A5)}$$

Note that the observation information matrix (5) combines the information from the forecast uncertainty (e.g., $\mathbf{P}_f$) and observation uncertainty (e.g., $\mathbf{R}$). The eigenvalue decomposition (EVD) of the matrix $\mathbf{C}$ reveals that the eigenvalues define the DOF for the signal, a useful flow-dependent diagnostic counting the number of independent pieces of information in the data assimilation.

The matrix inversion in (3) is achieved by performing an EVD,

$$\mathbf{I}_{N_E} + \mathbf{C}(\mathbf{x}^f) = \mathbf{V}\mathbf{\Lambda}\mathbf{V}^{\mathrm{T}}, \tag{A6}$$

where $\mathbf{V}$ is the matrix of eigenvectors, and $\mathbf{\Lambda}$ is a diagonal matrix of eigenvalues. Finally, the inverse square root is calculated such that

$$\mathbf{G} = \mathbf{P}_f^{1/2}\mathbf{V}\mathbf{\Lambda}^{-1/2}\mathbf{V}^{\mathrm{T}}. \tag{A7}$$

Note that the EVD is performed on an $N_E \times N_E$ matrix with $N_E \sim O(10^2)$, thus the computational requirements are not very demanding. Since the eigenvalues λ_i are all positive and cannot be smaller than one [e.g., (6)], the inverse in (3) is well defined. Finally, the square-root analysis error covariance calculated at the optimal point (analysis $\mathbf{x}^a$) using the formulation (3) is given by

$$\mathbf{P}_a^{1/2} = \mathbf{P}_f^{1/2}\left\{\mathbf{I}_{N_E} + [\mathbf{Z}(\mathbf{x}^a)]^{\mathrm{T}}\mathbf{Z}(\mathbf{x}^a)\right\}^{-1/2}, \tag{A8}$$

where the matrix $\mathbf{Z}(\mathbf{x}^a)$ is the observation perturbation matrix calculated at the optimal point $\mathbf{x}^a$. The column vectors of the square-root analysis error covariance (8) are then used as perturbations to the analysis for the next assimilation cycle, as indicated by (2).

REFERENCES

Aksoy, A., D. C. Dowell, and C. Snyder, 2009: A multicase comparative assessment of the ensemble Kalman filter for assimilation of radar observations. Part I: Storm-scale analysis. *Mon. Wea. Rev.,* **137,** 1805–1824.

Andersson, E., and Coauthors, 2005: Assimilation and modeling of the atmospheric hydrological cycle in the ECMWF forecasting system. *Bull. Amer. Meteor. Soc.,* **86,** 387–402.

Arndt, D. S., J. B. Basara, R. A. McPherson, B. G. Illston, G. D. McManus, and D. B. Demko, 2009: Observations of the overland reintensification of Tropical Storm Erin (2007). *Bull. Amer. Meteor. Soc.,* **90,** 1079–1093.

Bauer, P., P. Lopez, A. Benedetti, D. Salmond, and E. Moreau, 2006a: Implementation of 1D+4D-Var assimilation of precipitation-affected microwave radiances at ECMWF. I: 1D-Var. *Quart. J. Roy. Meteor. Soc.,* **132,** 2277–2306.

——, ——, ——, ——, S. Saarinen, and M. Bonazzola, 2006b: Implementation of 1D+4D-Var assimilation of precipitation-affected microwave radiances in precipitation at ECMWF. II: 4D-Var. *Quart. J. Roy. Meteor. Soc.,* **132,** 2307–2332.

Eito, H., and K. Aonashi, 2009: Verification of hydrometeor properties simulated by a cloud-resolving model using a passive microwave satellite and ground-based radar observations for a rainfall system associated with the Baiu front. *J. Meteor. Soc. Japan,* **87A,** 425–446.

Errico, R., J.-F. Mahfouf, and P. Bauer, 2007: Issues regarding the assimilation of cloud and precipitation data. *J. Atmos. Sci.,* **64,** 3785–3798.

Hou, A. Y., and S. Q. Zhang, 2007: Assimilation of precipitation information using column model physics as a weak constraint. *J. Atmos. Sci.,* **64,** 3865–3878.

Huffman, G. J., and Coauthors, 2007: The TRMM Multisatellite Precipitation Analysis (TMPA): Quasi-global, multiyear, combined-sensor precipitation estimates at fine scales. *J. Hydrometeor.,* **8,** 38–55.

Hunt, B. R., E. J. Kostelich, and I. Szunyogh, 2007: Efficient data assimilation for spatiotemporal chaos: A local ensemble transform Kalman filter. *Physica D,* **230,** 112–126.

Knabb, R. D., 2008: Tropical Storm Erin. National Hurricane Center, 17 pp. [Available online at http://www.nhc.noaa.gov/pdf/TCR-AL052007_Erin.pdf.]

Kummerow, C. D., and Coauthors, 2001: The evolution of the Goddard profiling algorithm (GPROF) for rainfall estimation from passive microwave sensors. *J. Appl. Meteor.,* **40,** 1801–1820.

Liu, H., J. Anderson, Y. H. Kuo, C. Snyder, and A. Caya, 2008: Evaluation of a nonlocal quasi-phase observation operator in assimilation of CHAMP radio occultation refractivity with WRF. *Mon. Wea. Rev.,* **136,** 242–256.

Lopez, P., 2007: Cloud and precipitation parameterizations in modeling and variational data assimilation: A review. *J. Atmos. Sci.,* **64,** 3766–3784.

Luenberger, D. L., 1984: *Linear and Non-Linear Programming*. 2nd ed. Addison-Wesley, 491 pp.

Macpherson, B., 2001: Operational experience with rainfall data in the Met Office mesoscale model. *Meteor. Atmos. Phys.,* **76,** 3–8.

Matsui, T., and Coauthors, 2008: Goddard Satellite Data Simulation Unit: A comprehensive multi-sensor satellite simulator for supporting satellite missions. *Eos, Trans. Amer. Geophys. Union,* **89** (Fall Meet. Suppl.), Abstract A31E-0159.

——, and Coauthors, 2009: Evaluation of long-term cloud-resolving model simulations using satellite radiance observations and multifrequency satellite simulators. *J. Atmos. Oceanic Technol.,* **26,** 1261–1274.

Menard, R., S. E. Cohn, L.-P. Chang, and P. M. Lyster, 2000: Assimilation of stratospheric chemical tracer observations using a Kalman filter. Part I: Formulation. *Mon. Wea. Rev.,* **128,** 2654–2671.

Meng, Z., and F. Zhang, 2008: Tests of an ensemble Kalman filter for mesoscale and regional-scale data assimilation. Part IV: Comparison with 3DVAR in a month-long experiment. *Mon. Wea. Rev.,* **136,** 3672–3682.

Miyoshi, T., and S. Yamane, 2007: Local ensemble transform Kalman filtering with an AGCM at a T159/L48 resolution. *Mon. Wea. Rev.,* **135,** 3841–3861.

Olson, W. S., and C. D. Kummerow, 1996: Simulated retrieval of precipitation profiles from TRMM Microwave Imager and precipitation radar data. Preprints, *Eighth Conf. on Saltellite Meteorology and Oceanography,* Atlanta, GA, Amer. Meteor. Soc., 248–251.

——, and Coauthors, 2006: Precipitation and latent heating distributions from satellite passive microwave radiometry. Part I: Improved method and uncertainties. *J. Appl. Meteor. Climatol.,* **45,** 702–720.

Redelsperger, J.-L., and Coauthors, 2000: A GCSS model intercomparison for a tropical squall line observed during TOGA-COARE. Part I: Cloud-resolving models. *Quart. J. Roy. Meteor. Soc.,* **126,** 823–864.

Skamarock, W. C., J. B. Klemp, J. Dudhia, D. O. Gill, D. M. Barker, W. Wang, and J. G. Powers, 2005: A description of the advanced research WRF version 2. NCAR Tech. Note NCAR/TN-468+STR, 88 pp.

Tao, W. K., 2003: Goddard Cumulus Ensemble (GCE) model: Application for understanding precipitation processes. *Cloud*

Systems, Hurricanes, and the Tropical Rainfall Measuring Mission (TRMM): A Tribute to Dr. Joanne Simpson, Meteor. Monogr., No. 51, Amer. Meteor. Soc., 103–108.

Tong, M., and M. Xue, 2005: Ensemble Kalman filter assimilation of Doppler radar data with compressible nonhydrostatic model: OSS experiments. *Mon. Wea. Rev.,* **133,** 1789–1807.

Treadon, R. E., H.-L. Pan, W.-S. Wu, Y. Lin, W. S. Olson, and R. J. Kuligowski, 2002: Global and regional moisture analyses at NCEP. *Proc. ECMWF/GEWEX Workshop on Humidity Analysis,* Reading, United Kingdom, European Centre for Medium-Range Weather Forecasts, 33–47.

Tsuyuki, T., K. Koisumi, and Y. Ishikawa, 2002: The JMA mesoscale 4D-Var system and assimilation of precipitation and moisture data. *Proc. ECMWF/GEWEX Workshop on Humidity Analysis,* Reading, United Kingdom, European Centre for Medium-Range Weather Forecasts, 59–67.

Vukicevic, T., T. Greenwald, M. Zupanski, D. Zupanski, T. Vonder Haar, and A. S. Jones, 2004: Mesoscale cloud state estimation from visible and infrared satellite radiances. *Mon. Wea. Rev.,* **132,** 3066–3077.

——, M. Sengupta, A. S. Jones, and T. Vonder Haar, 2006: Cloud-resolving data assimilation: Information content of IR window observations and uncertainties in estimation. *J. Atmos. Sci.,* **63,** 901–919.

Whitaker, J. S., T. M. Hamill, X. Wei, Y. Song, and Z. Toth, 2008: Ensemble data assimilation with the NCEP global forecast system. *Mon. Wea. Rev.,* **136,** 463–482.

Wilheit, T., C. Kummerow, and R. Ferraro, 2003: Rainfall algorithms for AMSR-E. *IEEE Trans. Geosci. Remote Sens.,* **41,** 204–213.

Wu, W.-S., R. J. Purser, and D. F. Parrish, 2002: Three-dimensional variational analysis with spatially inhomogeneous covariances. *Mon. Wea. Rev.,* **130,** 2905–2916.

Yang, S.-C., E. Kalnay, B. Hunt, and N. E. Bowler, 2009: Weight interpolation for efficient data assimilation with the local ensemble transform Kalman filter. *Quart. J. Roy. Meteor. Soc.,* **135,** 251–262.

Zhang, S. Q., D. Zupanski, A. Y. Hou, and M. Zupanski, 2008: Application of an ensemble smoother to precipitation assimilation. *Geophysical Research Abstracts,* Vol. 10, Abstract EGU2008-A-04209.

Zhou, Y. P., and Coauthors, 2007: Use of high-resolution satellite observations to evaluate cloud and precipitation statistics from cloud-resolving model simulations. Part I: South China Sea Monsoon Experiment. *J. Atmos. Sci.,* **64,** 4309–4329.

Zupanski, D., M. Zupanski, L. Grasso, R. Brummer, I. Jankov, D. Lindsey, M. Sengupta, and M. DeMaria, 2010: Assimilating synthetic GOES-R radiances in cloudy conditions using an ensemble-based method. *Int. J. Remote Sens.,* in press.

Zupanski, M., 2005: Maximum likelihood ensemble filter: Theoretical aspects. *Mon. Wea. Rev.,* **133,** 1710–1726.

——, I. M. Navon, and D. Zupanski, 2008: The maximum likelihood ensemble filter as a nondifferentiable minimization algorithm. *Quart. J. Roy. Meteor. Soc.,* **134,** 1039–1050.